

Supporting Information

Bifunctional High-Entropy Alloy Electrocatalysts for Stable Overall Water Splitting under Industrial-Level Current Densities

Yu Zhang^a, Qiang Wan^{b,}, Liqiu Huang^a, Tao Jiang^a, Shixin Wu^a, Derun Li^{a,*}, Yichao Liu^a, Hengyi Wu^a, Feng Ren^{a,*}*

^aSchool of Physics and Technology, Center for Ion Beam Application, Hubei Key Laboratory of Nuclear Solid Physics, Wuhan University, Wuhan 430072, China
E-mail: fren@whu.edu.cn

^bCollege of Engineering, Huazhong Agricultural University, Wuhan 430070, China

^cSchool of Materials Science and Engineering, Hubei Normal University, Huangshi 435002, China

Keywords: High entropy alloy; bifunctional; electrocatalysis

wanqiang0915@mail.hzau.edu.cn; drli@hbnu.edu.cn; fren@whu.edu.cn

1. Experimental Section

1.1 Preparation of FeCoNiCrMn HEA/NM

Atmospheric plasma spraying was carried out using FeCoCrNiMn high-entropy powder with a purity of 99.99% and a powder size of 300 mesh. A nickel mesh served as the spraying substrate. Prior to the spraying process, the oxide film on the surface of the nickel mesh was removed via sandblasting. For sandblasting, white corundum sand was selected, with a sandblasting pressure set at 0.08 MPa, and double sided sandblasting was implemented.

The nickel mesh substrate was vertically fixed in front of the spray gun. By adjusting parameters such as the spraying power, spraying distance, and gun travel speed (as

detailed in Table 1), the coating was prepared. Samples were sprayed on both sides of the substrate.

Table S1. Spraying process parameters

Power	Argon flow	Hydrogen flow	Powder feeding gas	Spray distance	Gun speed
40 kW	40 L/min	3 L/min	8 L/min	20 cm	12 m/min

1.2 Characterization

Field-emission scanning electron microscope (FESEM) was performed on the Hitachi S-4800. TEM and HRTEM images were characterized by JEM-F200 at 200 kV. XRD patterns were obtained from a Smart Lab 3KW with Cu K α irradiation. XPS was performed on a Thermo Scientific ESCALAB 250Xi system. Raman spectra were carried out on LabRAM HR Evolution.

1.3 Electrochemical Measurements

All electrochemical measurements were performed on an electrochemical workstation (CHI 760E, CH Instruments Inc., Shanghai). Hg/HgO electrode was used as the reference electrode and a carbon rod as the counter electrode. OER performances were measured by performing LSV (scan rate of 0.5 mV s⁻¹) in O₂ saturated 1 M KOH (pH = \approx 14) solution and HER performances were in 1.0 M KOH, and all initial data were corrected against the ohmic potential drop with 85% iR compensation unless otherwise noted. All the potentials reported for HER and OER were converted to the potential versus RHE according to $E_{\text{versus RHE}} = E_{\text{versus Hg/HgO}} + E^{\circ} \text{Hg/HgO} + 0.059 \text{ pH}$. EIS test was carried out in the range of 100 kHz to 0.001 Hz at the overpotential of 290 mV (versus RHE) with an AC amplitude of 10 mV. The long-time stability was quantified by recording a chronopotentiometry technique for three-electrode and two-electrode systems. Meanwhile, C_{dl} serves as an estimate of the ECSA of the solid-liquid interface as the relative ECSA is proportional to C_{dl} . The ECSA values were calculated based on the following equation: $\text{ECSA} = C_{dl}/C_s$. Here, $C_s = 0.04 \text{ mF cm}^{-2}$.

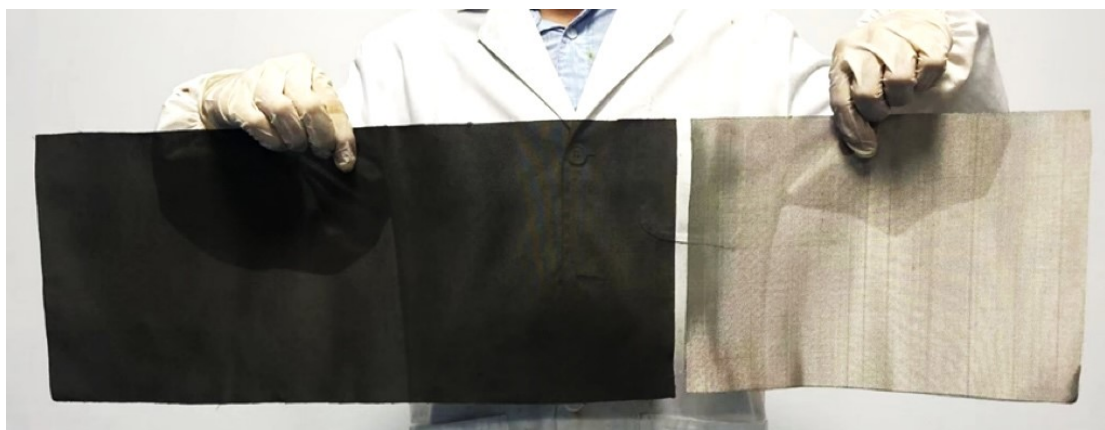


Figure S1. Digital photos of FeCoNiCrMn HEA/NM catalysts (left) and the pristine Ni mesh (right).

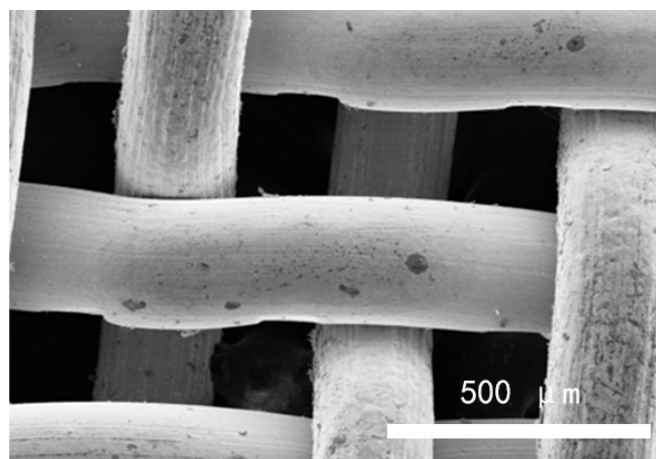


Figure S2. SEM image of the pristine nickel mesh.

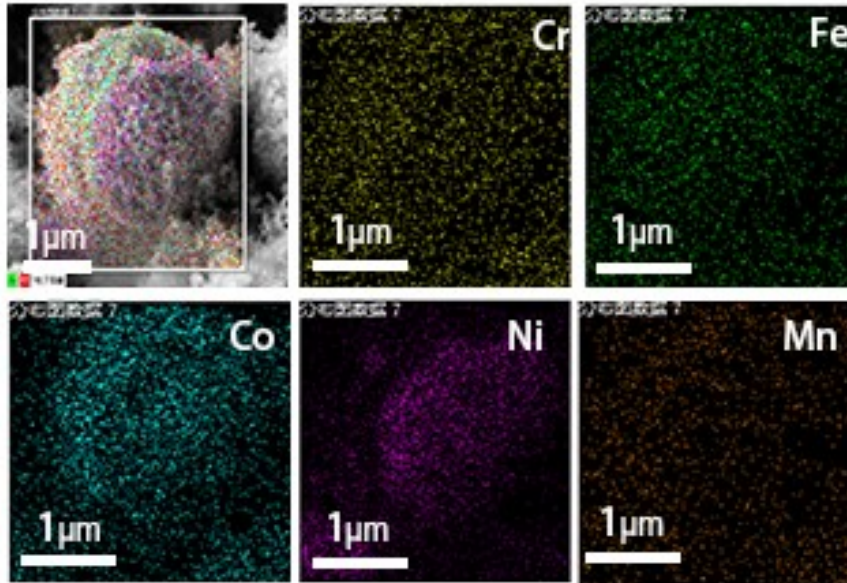


Figure S3. SEM and EDS-mapping images of FeCoNiCrMn HEA/NM catalyst.

Table S2. The graph showing the elemental composition ratio.

Element	At%
Ni	29.86%
Co	27.62%
Mn	16.16%
Cr	15.10%
Fe	11.26%

Table S3. Calculated configurational entropy of mixing of FeCoNiCrMn HEA/NM.

Sample	ΔS_{mix}
FeCoNiCrMn HEA/NM	1.54R

The calculation of mixed entropy for HEA/ NM could be made following the equation:

$$\Delta S_{mix} = -R \sum_{i=1}^n X_i \ln X_i$$

Where ΔS_{mix} is the configurational entropy of mixing, R is the gas constant, X_i is the molar ratio of component i, and n is the total number of elements involved.

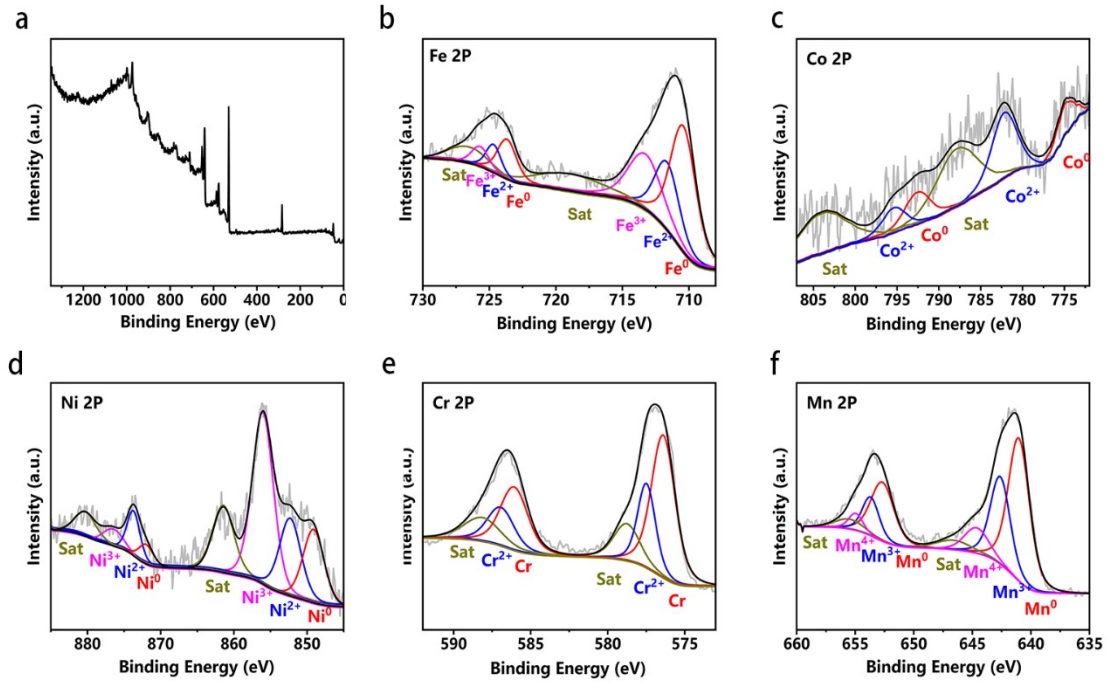


Fig S4. XPS spectra of the FeCoNiCrMn HEA/NM.

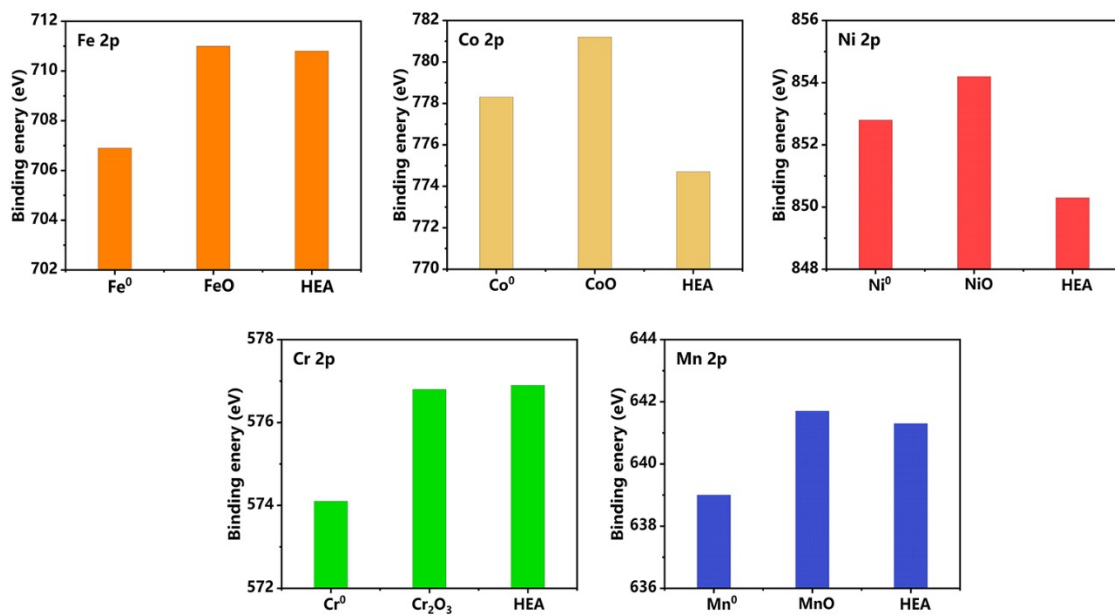


Figure S5. A comparison of the binding energies of the FeCoNiCrMn HEA/NM,

metals, and metal oxides for each element.

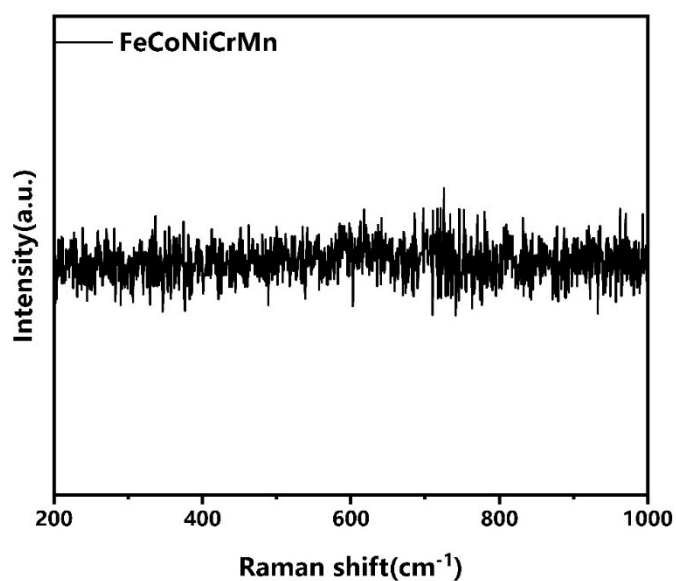


Figure S6. Raman spectrum of FeCoNiCrMn HEA/NM.

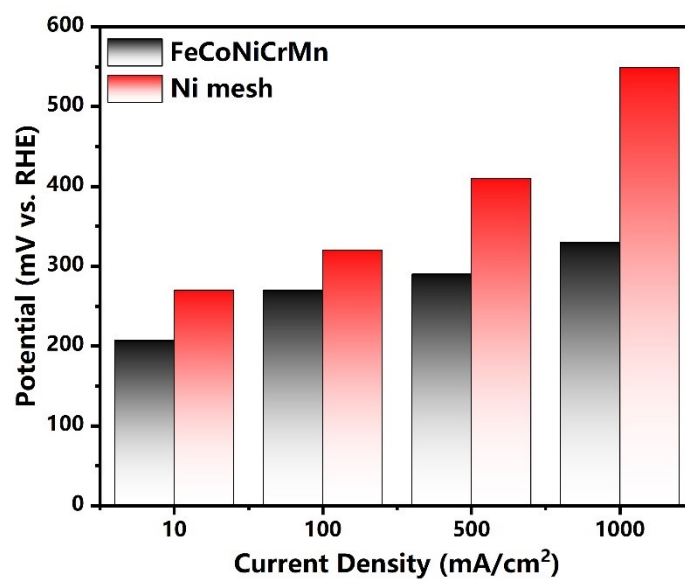


Figure S7. Comparison of OER performance between FeCoNiCrMn HEA/NM and Nickel mesh.

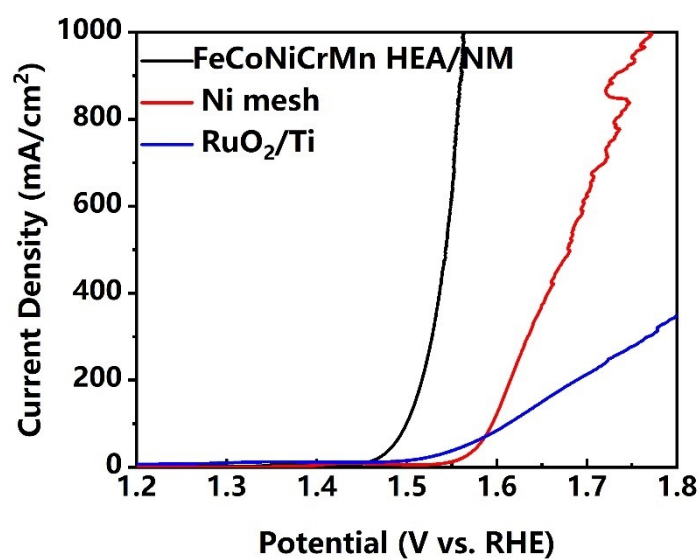


Fig. S8. OER Polarization curves of FeCoNiCrMn HEA/NM, Ni mesh and RuO₂/Ti.

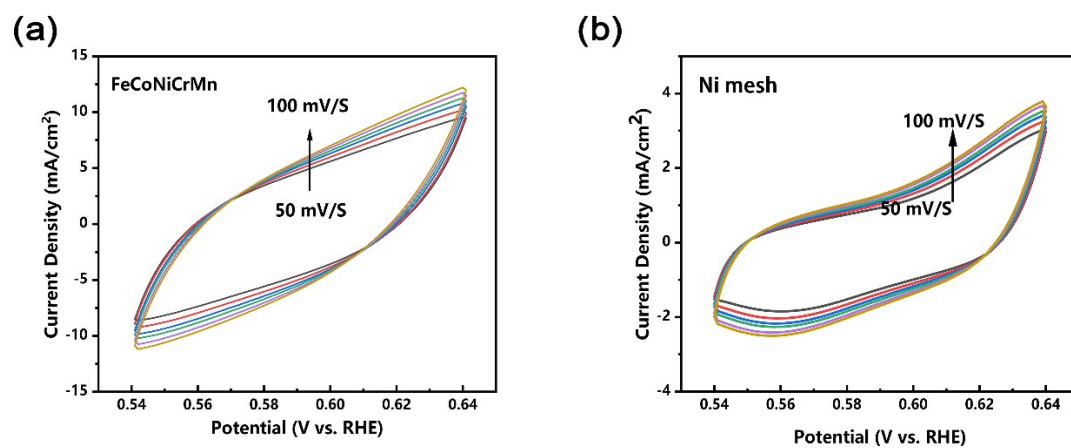


Figure S9. The CV curve of FeCoNiCrMn HEA/NM (a) and Ni mesh (b).

Table S4. Resistance value obtained from electronic equivalent circuit simulation

	$R_s(\Omega)$	$R_{ct}(\Omega)$	CPE-T	CPE-P
FeCoNiCrMn HEA/NM	1.05	1.87	0.03	0.77
Ni mesh	1.03	3.93	0.06	0.83

Table S5. Comparison of OER performance of FeCoNiCrMn HEA catalyst with recently reported HEAs electrocatalysts in 1 M KOH alkaline media.

Catalyst	η_{10} (mV)	Tafel slope (mV/dec)	Stability	Refs.
FeCoNiCrMn HEA/NM	207	40	1000 h @ 1000mA cm⁻²	This work
FeCoNiCuMoB	201	41.3	30 h @ 100 mA cm ⁻²	1
FeCoNiMnRu-HCB _{0.5}	229	105	20 h @ 20 mA cm ⁻²	2
FeCoCrMnNi HEA	231	66	100 h @ 100mA cm ⁻²	3
Co-Fe-Ga-Ni-Zn	370	71	10 h @ 10mA cm ⁻²	4
MnFeCoNi HEA	302	83.7	20 h @ 10mA cm ⁻²	5
FeCoNiMnCr HEA-HEO/CNT	261	42.2	240 h @ 100mA cm ⁻²	6
FeNiMnCrCu HEA	317	58	10 h @ 26 mA cm ⁻²	7
AlCrCuFeNi HEAs	270	77.5	35 h @ 17.5 mA cm ⁻²	8
HF-CoCrFeNiAl HEA	265	56.8	10 h @ 10 mA cm ⁻²	9
MnFeCoNiCu	263	43	24 h @ 10 mA cm ⁻²	10
FeCoNiMo HEA	250	42.5	65 h @ 10 mA cm ⁻²	11
MnFeCoNiCu HE-MOF-ST	293	81	48 h @ 10mA cm ⁻²	12
CoCrFeMnNiP HEMP	320	60.8	24 h @ 10mA cm ⁻²	13
Fe-Cr-Co-Ni-Cu HE-LDHs- Ar-20	330	63.7	24 h @ 10 mA cm ⁻²	14
(Fe _{0.73} Cr _{0.71} Co _{0.78} Ni _{0.81} Al _{0.1}) O _{4.01} HEO	381	97.4	120 h @ 10 mA cm ⁻²	15

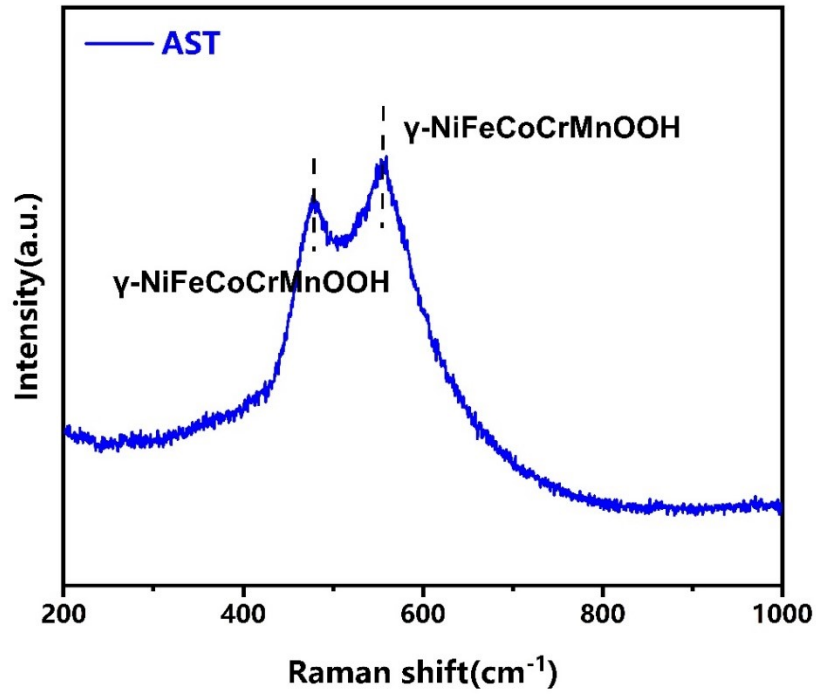


Figure S10. Raman spectrum of the after the stability test- catalyst.

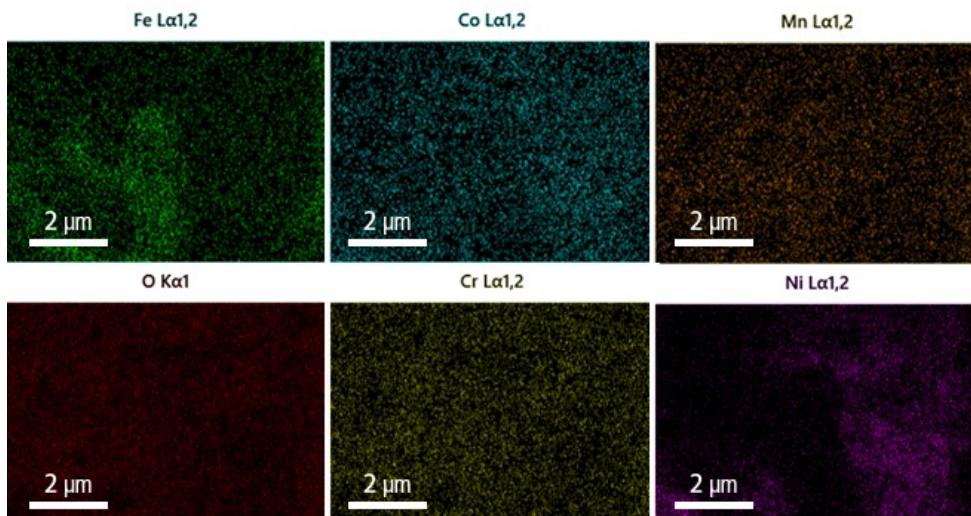


Fig. S11.EDS-mapping images of FeCoNiCrMn HEA/NM catalyst after OER stability test.

Table S6. The graph showing the elemental composition ratio after OER stability test.

Element	At%
Ni	10.3%
Co	7.0%
Mn	13.5%
Cr	6.0%
Fe	11.7%
O	51.5%

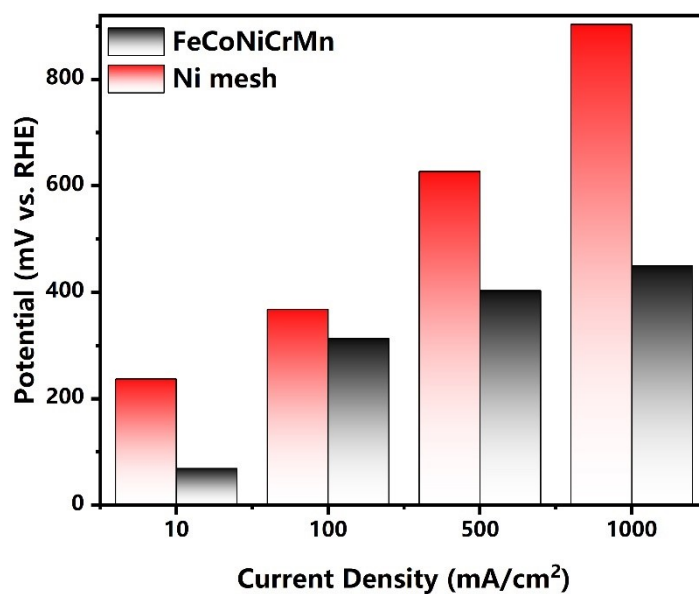


Figure S12. Comparison of HER performance between FeCoNiCrMn HEA/NM and nickel mesh.

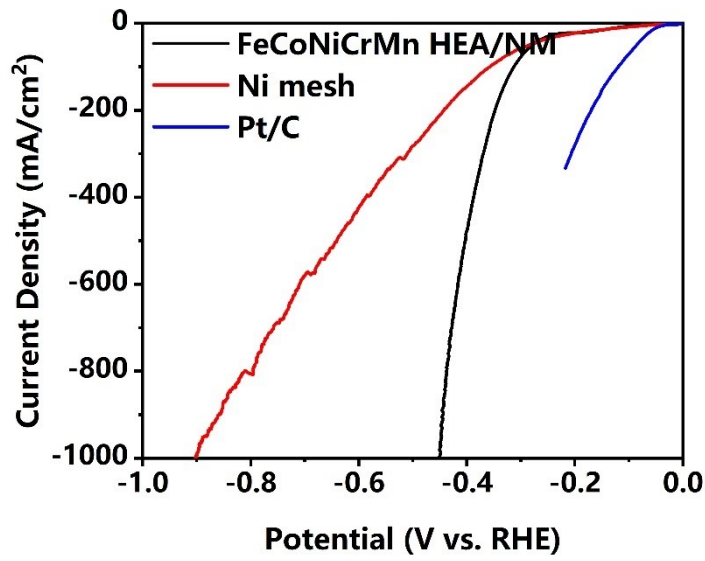


Fig. S13. HER Polarization curves of FeCoNiCrMn HEA/NM, Ni mesh and Pt/Ti.

Table S7. Resistance value obtained from electronic equivalent circuit simulation

	$R_s(\Omega)$	$R_{ct}(\Omega)$	CPE-T	CPE-P
FeCoNiCrMn HEA/NM	1.02	0.77	0.04	0.75
NM	1.08	1.58	0.03	0.76

Table S8. Comparison of HER performance and stability of FeCoNiCrMn HEA

catalyst with recently reported HEAs electrocatalysts in alkaline media.

Catalyst	Electrolyte	$\eta_{10}(\text{mV})$	stability	Refs.
FeCoNiCrMn HEA/NM	1 M KOH	69	500 h at 1000 mA/cm²	This work
FeCoNiCuMoB HEA	1 M KOH	26	30 h at 100 mA/cm ²	1
PdPtRuRhAu HEA	0.5 M H ₂ SO ₄	70.07	90 h at 1000 mA/cm ²	16
FeCoNiMnRu-HCB _{0.5}	1 M KOH	42	20 h at 25 mA/cm ²	2
FeCoCrMnNi HEA	1 M KOH	168	/	3
FeCoNiAlTi HEI	1 M KOH	88.2	40 h at 200 mA/cm ²	17
CNF@PtIrFeNiCo	0.1 M KOH	59.8	5000 cycles	18
Co _x (VMnNiZn) _{1-x} PS ₃	1 M KOH	65.9	3000 cycles/	19
FeCoNiCuMnN	1 M KOH	184	50 h at 20 mA/cm ²	20
FeNiCoMnVO _x	1 M KOH	81	100 h at 10 mA/cm ²	21
CoCrFeNiMo	1 M KOH	156.7	14 h at 40 mA/cm ²	22
Cr _x MnFeNi	1 M KOH	180	36 h at 100 mA/cm ²	23
Al _{96.6} Fe _{1.42} Ni _{1.38} Mo _{0.2} Co _{0.2} C _{r0.2}	1 M KOH	110	/	24
FeCoNiCuPd	1 M KOH	29.7	36 h at 100 mA/cm ²	25
np-UHEA14	1 M KOH	42	15 h at 100 mA/cm ²	26
IrPdPtRhRu	1 M KOH	50		27

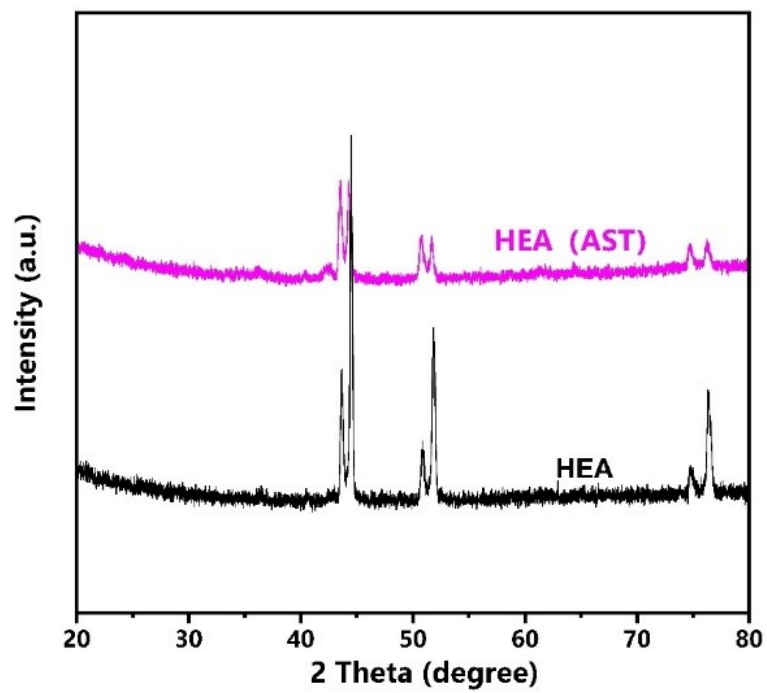


Figure S14. XRD patterns after HER stability test.

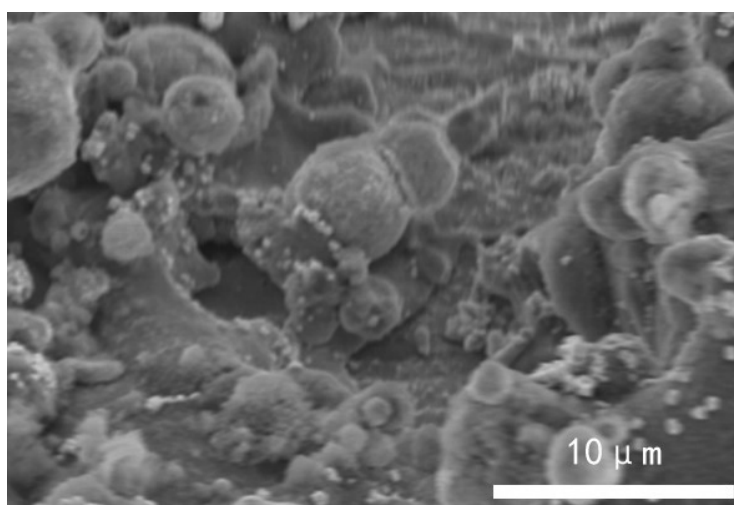


Figure S15. SEM images after HER stability test.

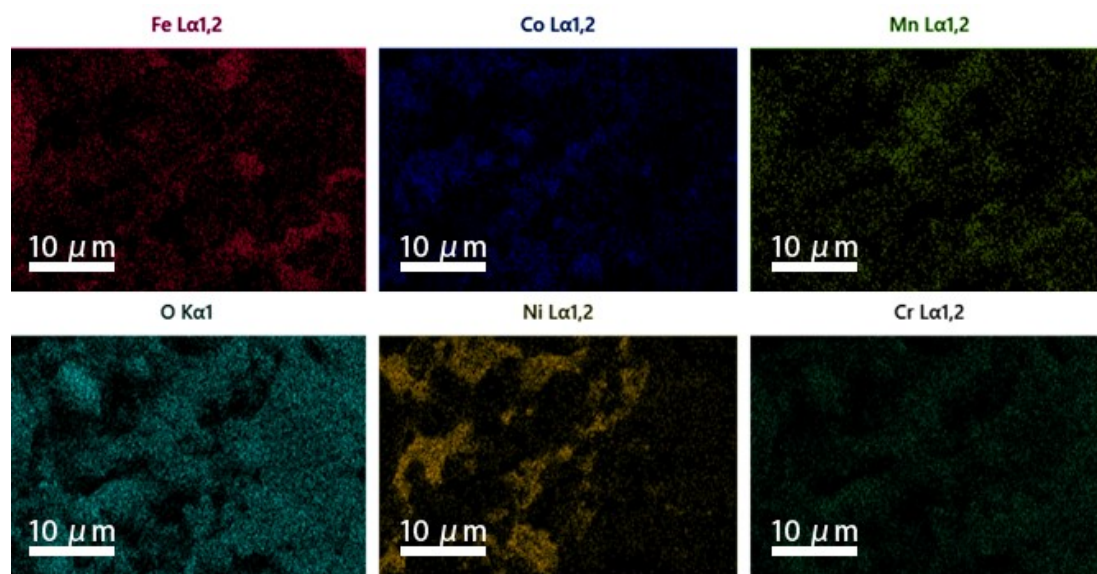


Fig. S16.EDS-mapping images of FeCoNiCrMn HEA/NM catalyst after OER stability test.

Table S9. The graph showing the elemental composition ratio after HER stability test.

Element	At%
Ni	15.1%
Co	5.7%
Mn	9.8%
Cr	18.1%
Fe	11.2%
O	40.1%

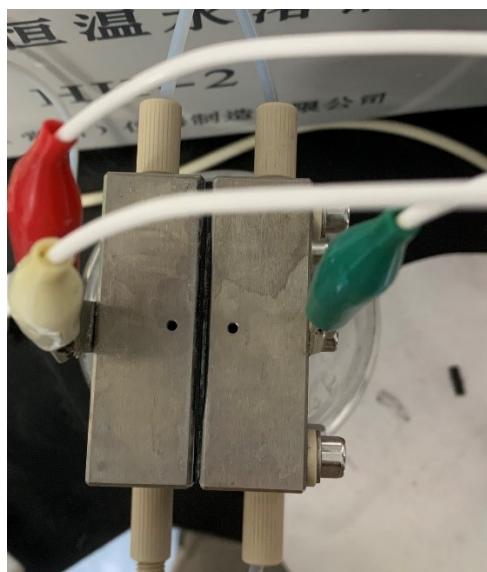


Figure S16. Diagram of the overall water splitting device.

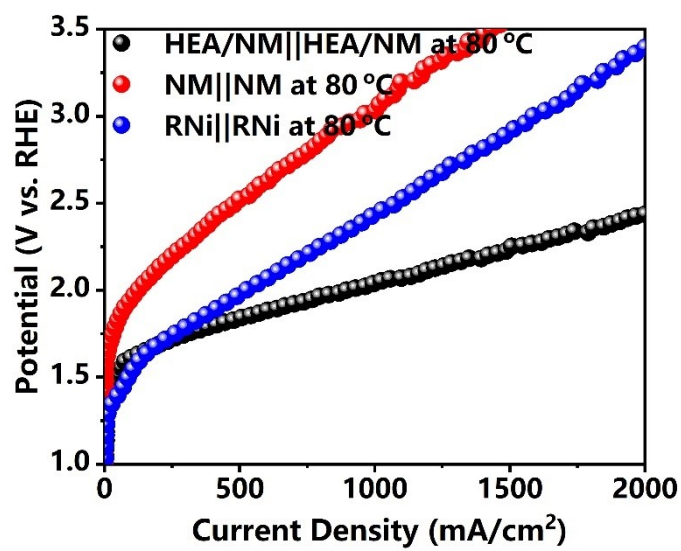


Figure S17. Overall water-splitting polarization curve at 80 °C.

References

- 1 S. Wang, H. Yan, W. Huo, A. Davydok, M. Zając, J. Stępień, H. Feng, Z. Xie, J. K. Shang, P. H. C. Camargo, J. Jiang and F. Fang, *Appl. Catal. B Environ. Energy*, 2025, 363, 124791.
- 2 L. Wang, C. Wang, Y. Mu, J. Fan, X. Yang, C. Yu, B. Guo and G. Zeng, *Fuel*, 2025, 391, 134800.
- 3 B. Wen, X. Zhao, Q. Dong, B. Li and X. Lyu, *J. Power Sources*, 2025, 627, 235804.
- 4 L. Sharma, N. K. Katiyar, A. Parui, R. Das, R. Kumar, C. S. Tiwary, A. K. Singh, A. Halder and K. Biswas, *Nano Res.*, 2022, 15, 4799–4806.
- 5 W. Dai, T. Lu and Y. Pan, *J. Power Sources*, 2019, 430, 104–111.
- 6 J. Hu, T. Guo, X. Zhong, J. Li, Y. Mei, C. Zhang, Y. Feng, M. Sun, L. Meng, Z. Wang, B. Huang, L. Zhang and Z. Wang, *Adv. Mater.*, 2024, 36, 2310918.
- 7 X. Cui, B. Zhang, C. Zeng and S. Guo, *MRS Commun.*, 2018, 8, 1230–1235.
- 8 L.-H. Liu, N. Li, M. Han, J.-R. Han and H.-Y. Liang, *Rare Met.*, 2022, 41, 125–131.
- 9 C.-X. Zhao, J.-N. Liu, B.-Q. Li, D. Ren, X. Chen, J. Yu and Q. Zhang, *Adv. Funct. Mater.*, 2020, 30, 2003619.
- 10 K. Huang, B. Zhang, J. Wu, T. Zhang, D. Peng, X. Cao, Z. Zhang, Z. Li and Y. Huang, *J. Mater. Chem. A*, 2020, 8, 11938–11947.
- 11 Y. Mei, Y. Feng, C. Zhang, Y. Zhang, Q. Qi and J. Hu, *ACS Catal.*, 2022, 12, 10808–10817.
- 12 X. Zhao, Z. Xue, W. Chen, X. Bai, R. Shi and T. Mu, *J. Mater. Chem. A*, 2019, 7, 26238–26242.
- 13 X. Zhao, Z. Xue, W. Chen, Y. Wang and T. Mu, *ChemSusChem*, 2020, 13, 2038–2042.
- 14 J. Li, X. Gu, J. Chang, D. Wu, F. Xu, K. Jiang and Z. Gao, *J. Colloid Interface Sci.*, 2022, 606, 1662–1672.
- 15 S. Zhao, H. Wu, R. Yin, W. Xuening, H. Zhong, Q. Fu, W. Wan, T. Cheng, Y. Shi, G. Cai, C. Jiang and F. Ren, *J. Alloys Compd.*, 2021, 868, 159108.

- 16 Q. Wang, Y. Qin, J. Xie, Y. Kong, Q. Sun, Z. Wei and S. Zhao, *Adv. Mater.*, 2025, 37, 2420173.
- 17 Z.-X. Cai, H. Goou, Y. Ito, T. Tokunaga, M. Miyauchi, H. Abe and T. Fujita, *Chem. Sci.*, 2021, 12, 11306–11315.
- 18 N. Yao, G. Wang, H. Jia, J. Yin, H. Cong, S. Chen and W. Luo, *Angew. Chem. Int. Ed.*, 2022, 61, e202117178.
- 19 R. Wang, J. Huang, X. Zhang, J. Han, Z. Zhang, T. Gao, L. Xu, S. Liu, P. Xu and B. Song, *ACS Nano*, 2022, 16, 3593–3603.
- 20 M. W. Glasscott, A. D. Pendergast, S. Goines, A. R. Bishop, A. T. Hoang, C. Renault and J. E. Dick, *Nat. Commun.*, 2019, 10, 2650.
- 21 Z. Jin, J. Lyu, Y.-L. Zhao, H. Li, X. Lin, G. Xie, X. Liu, J.-J. Kai and H.-J. Qiu, *ACS Mater. Lett.*, 2020, 2, 1698–1706.
- 22 X. Huo, X. Zuo, X. Wang, B. Xing and N. Zhang, *Chem. – Asian J.*, 2023, 18, e202300456.
- 23 Y. Wang, N. Gong, G. Niu, J. Ge, X. Tan, M. Zhang, H. Liu, H. Wu, T. L. Meng, H. Xie, K. Hippalgaonkar, Z. Liu and Y. Huang, *J. Alloys Compd.*, 2023, 960, 171039.
- 24 D. Li, C. Zhong, X.-L. Huo, F. Ren and Q. Zhou, *Chem. Commun.*, 2023, 59, 4209–4212.
- 25 S. Ding, Y. Sun, F. Lou, L. Yu, B. Xia, J. Duan, Y. Zhang and S. Chen, *J. Power Sources*, 2022, 520, 230873.
- 26 Z.-X. Cai, H. Goou, Y. Ito, T. Tokunaga, M. Miyauchi, H. Abe and T. Fujita, *Chem. Sci.*, 2021, 12, 11306–11315.
- 27 G. Lee, N.-A. Nguyen, V.-T. Nguyen, L. L. Larina, E. Chuluunbat, E. Park, J. Kim, H.-S. Choi and M. Keidar, *J. Solid State Chem.*, 2022, 314, 123388.